Hydration mechanics of sewage sludge ashes used as cement replacement

Mehdi Mejdi, Mickael Saillio, Thierry Chaussadent, Loïc Divet, Arezki Tagnit-Hamou

HYDRATION MECHANISMS OF SEWAGE SLUDGE ASHES USED AS CEMENT REPLACEMENT

Mehdi Mejdi[a,b], Mickael Saillio[a], Thierry Chaussadent[a], Loic Divet[a], and Arezki Tagnit-Hamou[b]

[a] Université Gustave Eiffel, MAST, CPDM, IFSTTAR F-77447 Marne-La-Vallée, France

[b] Département de Génie Civil, Université de Sherbrooke, Sherbrooke (Québec), J1K 2R1, Canada

Abstract

The influence of sewage sludge ash (SSA) on the hydration of Portland cement (OPC) was investigated in this study. Blending OPC with SSA was found to influence the kinetic of hydration, notably the alite dissolution. This retardation effect has been attributed to the presence of the orthophosphate ions (PO_4^{3-}). However, SSA releases only a small fraction of PO_4^{3-} into solution, which is deemed insufficient to precipitate calcium phosphates compounds on noticeable levels at least. On the other hand, an enhancement of the engineering-scale properties (i.e. mechanical and durability) and portlandite consumption are observed when SSA is used. This is explained by the formation of AFm phases, which leads to changes in the total volume of the solid and thus the properties of the systems. These experimental results were confirmed by thermodynamic modelling, showing that the additional alumina released by SSA results in the formation of higher amount of AFt and AFm phases.

Keywords

Sewage sludge ash, cement hydration, AFm phase, kinetics, phase assemblage

1. INTRODUCTION

Sewage sludge is an inevitable by-product produced during waste water treatment. Depending on its quality (with regards to pollutant concentrations), different methods can be used to dispose of this waste. However, due to the current environmental awareness, many of these disposal practices have been subject to more or less legal limitations: ocean dumping has been banned since 1998 for environmental reasons (Urban Waste Water Directive 98/15/EC), a cautionary application to soils as a fertilizer has been advocated by some countries for health concerns (Council Directive 86/278/EEC), and finally limits have been introduced for biodegradable wastes going to landfills in order to reduce the emissions of methane and carbon dioxide from these sites (Waste Landfill Directive 1999). Within this legislative context, incineration has become one of the most environmental friendly disposal options and has received increasing attention, particularly in Europe [1]. Nevertheless, the incineration process only diminishes the wastes weight by nearly 70% (≈70–90% by volume), generating residual sewage sludge ashes (SSA) as an ultimate by-product to deal with [2]. In the past decades, these ashes have been usually landfilled due the relatively low amounts generated each year (estimated of 1.2 Mt in 2004 in USA and Europe [3]). However, the rising amount of sludge being incinerated urges the search for alternative means to reuse or recycle the SSA.

The construction field has provided a brand new recovery channel for this waste through its use in bricks, tiles, ceramics, lightweight materials, aerated concrete, soil stabilization [2–17]. Recently, some studies have also suggested a potential use as replacement or in substitution to cement and reviewed the properties of the SSA-blended mortars and/or concretes from a technological and engineering point of view [2,3,18–25]. On the one hand, SSA tends to increase the water demand, to reduce the workability and to delay the setting of concrete and mortars. On the other hand, however, acceptable strength activity indexes for replacement rates below 20 wt.% (i.e. standard for pozzolanic activity) and a high consumption of portlandite (amounts of $Ca(OH)_2$ fixed) have been reported when the SSA are used. These observations have inferred to SSA the characteristic of being pozzolanic [19,21,23,26] and aroused the interest in its use as an alternative supplementary cementitious material (SCM).

Despites the promising results of the SSA as cement component, there is still little information available about its hydration mechanisms and its impact on the phase assemblage of the cementitious matrix. In addition to the low alumina and silica contents compared to conventional SCMs, several authors have reported the presence of phosphate in SSA, often in form of iron- or magnesium-bearing whitlockite (WH, $Ca_9(Mg,Fe)(PO_4)_6PO_3OH$) [3,26–29], calcium aluminium phosphates ($Ca_9(Al)(PO_4)_7$) [30], aluminium or iron phosphates ($(Al,Fe)PO_4$) [29–31], or hydroxyapatite (HAP, $Ca_5(PO_4)_3(OH)$) [28,29]. Hence, the composition of SSA makes its chemistry distinguishable from the cement based materials. Furthermore, the portlandite consumption and the compressive strength gains might be related to the

formation of other compounds than C-S-H (e.g. hydroxyapatite [22,26], or hydrogarnet [3]) and thus SSA cannot be simply considered as a pozzolanic SCM [26].

In this respect, the aim of this paper is to identify and quantify the changes in the hydration products upon the addition of SSA. First, the hydraulic and pozzolanic reactivity of SSA is investigated using isothermal calorimetry and X-ray diffraction. Then, the effects of replacing 10 and 20 wt.% of the cement by SSA are investigated in terms of macro-scale properties and phase assemblage of cementitious matrix. Finally, thermodynamic modelling was employed to validate the experimental observations.

2. Materials and methods

2.1 Materials

In this work, the cement pastes and mortars were prepared using a commercially available Portland Cement (OPC) from Ciment Quebec and conforming to ASTM C150 [32], a class F fly ash (FA) from Lafarge, and a sewage sludge ash (SSA) obtained by incinerating an urban sewage sludge (from Grenoble region, France) in a fluidized bed furnace at 850 °C. The chemical and physical properties of the raw materials and the characterisation technics employed are summarized in Table 1. Besides, Table 2 shows the mineral composition obtained by X-ray diffraction combined with the Rietveld refinement, whereas Fig. 1 displays the particle size distributions determined by laser granulometry of the aforementioned materials.

Table 1. Chemical and physical characterizations of the studied materials OPC, SSA, FA.

	OPC	***SSA***	***FA***	***Method/Instrument***
SiO_2	19.5	28.6	46.4	
CaO	60.5	20.1	4.5	
Al_2O_3	4.4	17.6	23.2	
Fe_2O_3	2.6	4.4	16.5	
Na_2O	0.3	0.6	0.8	
K_2O	0.9	1.9	1.9	
P_2O_5	0.9	19.5	0.4	Phillips PW-2600 X Fluorescence
SO_3	4.0	2.0	0.7	Spectrometer
Mn_2O_3	0.1	0.0	0.0	
MgO	2.9	2.3	1.0	
TiO_2	0.2	1.5	1.1	
Cr_2O_3	0.0	0.1	0.0	
SrO	0.2	0.1	0.1	
ZnO	0.0	0.2	0.2	
Loss On Ignition (LOI)	2.7	0.7	2.7	LOI at 1000°C
Equivalent alkali	0.9	1.8	2.1	Na_2O_{eq} (%) = Na_2O+0,658 x K_2O (%)

D_{50} (µm)	16.3	30.8	14.4	Malvern's Mastersizer 2000 laser granulometer
Density	3.11	2.62	2.51	Pycnometry
Blaine (m^2/kg)	395	845	387	Blaine fineness
BET (m^2/g)	1.26	5.2	-	Micromeritics ASAP2010
Lime fixed (mg per g)	-	362	512	Pozzolanic test NF P18-513

90

Table 2. Mineral composition of the studied materials.

	Chemical formula	***OPC***	***SSA***	***FA***
Alite	Ca_3SiO_5	52.1		
Belite	Ca_2SiO_4	11.5		0.8
Aluminate	$Ca_3Al_2O_6$	4.3		
Ferrite	Ca_3FeAlO_5	8.6		
Lime	CaO		0.9	
Portlandite	$Ca(OH)_2$			1.1
Periclase	MgO	0.6		0.5
Gypsum	$CaSO_4{\cdot}2H_2O$	3.4		2.0
Bassanite	$CaSO_4{\cdot}1/2H_2O$	2.6		
Anhydrite	γ–$CaSO_4$	0.3	3.1	0.8
Apthitalitite	$K_{2.25}Na_{1.75}(SO_4)_2$	0.2		
Calcite	$CaCO_3$	3.3		2.7
Quartz	SiO_2	0.3	14.7	9.1
Hematite	Fe_2O_3		0.4	0.5
Mullite	$Al_{4.5}Si_{1.5}O_{9.75}$			1.7
Microcline - Feldspars	$KAlSi_3O_8$		4.4	
Whitlockite	$Ca_7Mg_2P_6O_{24}$		27.9	
Hydroxyapatite	$Ca_5(PO_4)_3(OH)$		0.3	
Amorphous/unidentified		12.8	48.3	80.6

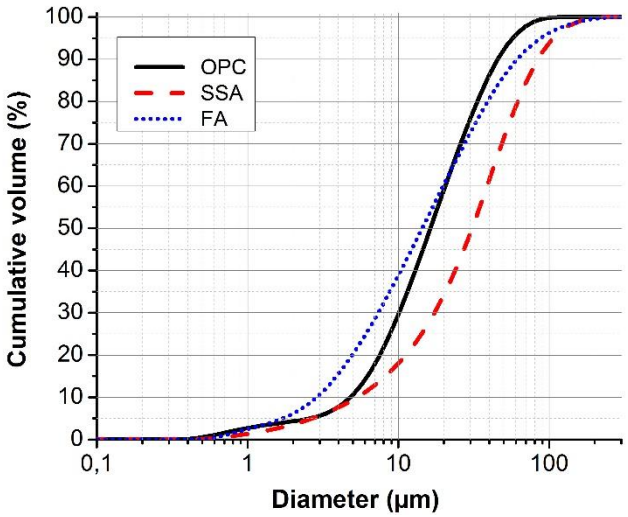

91

Fig. 1. Particle size distribution of OPC, SSA and FA.

2.2 Methods

2.2.1 Samples preparation

The hydraulic and pozzolanic activities of SSA were evaluated through mixture with water, KOH solution, and calcium hydroxide+water (NF P18-513 2012) [33]. The water to solid mass ratio was fixed to 1 to achieve a good rheology of the pastes. For the CH-SSA systems, two mass proportions were used 50 wt.% SSA and 25 wt.% SSA, which in the following will be respectively referred to as 50SSA50CH and 25SSA75CH. All the mixtures were prepared using a propeller mixer (2 min, 2000 rpm).

Standard mortar cubes (5x5x5 cm) were prepared with a binder:sand:water ratio (by weight) of 1:2.75:0.485 according to ASTM C109. The blended cements were prepared by replacing commercial Ordinary Portland Cement (OPC) with sewage sludge ash (SSA) according to the following percentages: 0, 10, and 20% by weight. After demolding, the specimens were immersed in a lime-saturated solution until the age of testing. The blended mortar cubes were used to evaluate the effect of SSA on compressive strength and electrical resistivity, while the mortars with neat OPC were used, for comparison purpose, as control samples.

The phase changes due to the inclusion of SSA were investigated using cement pastes at a water to binder ratio of 0.485. Two replacement levels (10 and 20 wt. %) were used for the SSA-blended systems. The pastes were cast in plastic containers, sealed, and stored in a desiccator with soda-lime to avoid CO_2 contamination. Before the testing ages of 1, 3, 7, 14, 28, 56, 91, 180, and 300 days, the hardened pastes were manually ground (d_{50}≈40 µm) and the hydration was immediately stopped by placing the sample in isopropanol for 15 min. Afterwards, the isopropanol was filtered and removed by solvent exchange with diethyl ether followed by a short vacuum drying process [34,35].

2.2.2 Isothermal calorimetry

The hydration heat evolution of the control and the SSA-blended pastes (weight replacements of 10, 20, and 30%) was analysed using a TAM Air isothermal calorimeter (TA instruments). For each mixture, a sample of about 4.5 g at a water to binder weight ratio of 0.485 was placed in an ampoule and inserted into the calorimeter cell. The heat measurements were collected continuously during the first week (7 days) of hydration.

2.2.3 Thermogravimetric analyses (TGA)

Thermogravimetric investigations were carried out with a TA instrument SDT Q600 over a temperature range of 30–1000°C at a heating rate of 20 °C/min. The measurements were

performed on about 50 mg of the ground sample (after the hydration stoppage), placed in a 150 µL alumina crucible. Nitrogen with a flow of 50 mL/min was used as a purging gas. TGA was used to determine the chemically bound water and the mass loss corresponding to the portlandite decomposition.

2.2.4 X-ray diffraction analyses (XRD)

X-ray powder diffraction was used to identify the mineralogical composition of both raw materials and hydrated pastes. X-ray Data were collected using a PANalytical X'pert Pro MRD diffractometer equipped with a PIXcel 1D detector. The analyses were performed on back-loaded samples in a Bragg-Brentano (θ-2θ) geometry, using Soller slits of 0.04 rad. Further details concerning the XRD operating parameters are reported in Table 3. On the other hand, an Alfa Aesar α-Al_2O_3 corundum, calibrated to 98.2% crystalline content using a certified corundum standard from the National Institute of Standards and Technology (NIST 676a), was used as an external standard to quantify the amorphous content of the samples [36]. The standard was scanned frequently to take into account the decay of the X-ray tube.

Table 3. Instrumental settings for X-ray data collection

	Powder XRD
Current/Voltage	50 mA / 40 kV
Angular range	5 to 70° 2θ
Detector's active length	3.347° 2θ
Step size	0.0263° 2θ
Counting Time	176 s
Measurement time	30 min
Vertical spinning	8 rpm
Divergence slit	0.5°
Anti-Scatter slit	0.5°
Scan mode	Continuous

2.2.5 ^{27}Al nuclear magnetic resonance

^{27}Al NMR spectroscopy is a powerful tool to analyse the structure of both amorphous and crystalline materials, at a local scale. It provides insight on the geometrical configuration of the nucleus and the coordination of the atoms as a function of the chemical shift. ^{27}Al magic-angle spinning NMR (MAS NMR) spectra were performed at a frequency of 130.3 MHz using a Brucker Avance III (11.74 T magnetic field). The spectrometer was equipped with a 4 mm probe head operating at a spinning frequency of 11.5 KHz. The record was carried out with a pulse length of 1.5 µs and a relaxation delay of 5 s. The chemical shift was referenced using Al^{3+}_{aq} in a 0.1 M $AlCl_3$ aqueous solution.

3. Overview of sewage sludge ashes

3.1 Variability of the composition

The main elements present in SSAs as reported in the literature are silicon, aluminium, iron, calcium and phosphorus. Fig. 2 illustrates the variation range and average weight percentage of the major components of SSAs, compiled from former studies [2,3,7–9,15,19,21,30,31,37–56]. Given the wide range of variation of the oxides (e.g. ≈62 wt.% for SiO_2), it can be concluded that the sewage sludge ashes present a very high variability. Indeed, the composition of SSAs could be heavily influenced by several factors such as the type of the effluents (urban, industrial, etc.), the treatment processes (e.g. removal of phosphates [43]), the incineration process, etc. Fig. 2 also shows that the oxide composition of the SSA studied here fall into the average regions (except Fe_2O_3 and P_2O_5). Therefore, the SSA in this study might be considered representative of other SSAs to some extent. It should also be noted that the amount of oxides intervening in the pozzolanic reaction (SiO_2+Al_2O_3 < 50 wt.%) are low compared to conventional SCMs, with a significant part expected to be inert (in form of quartz and feldspars). On the other hand, SSA contains high levels of CaO, Al_2O_3 and P_2O_5, mainly in the form of calcium phosphates minerals (whitlockite). The presence of high amount of CaO is related to the use of lime in the water treatment process. Furthermore, other minor minerals have been observed such as hematite and anhydrite, in addition to a vitreous (or unidentified) phase of ≈48 wt.%, as shown in Fig. 3. Similar observations have been reported by Cyr and al. [3].

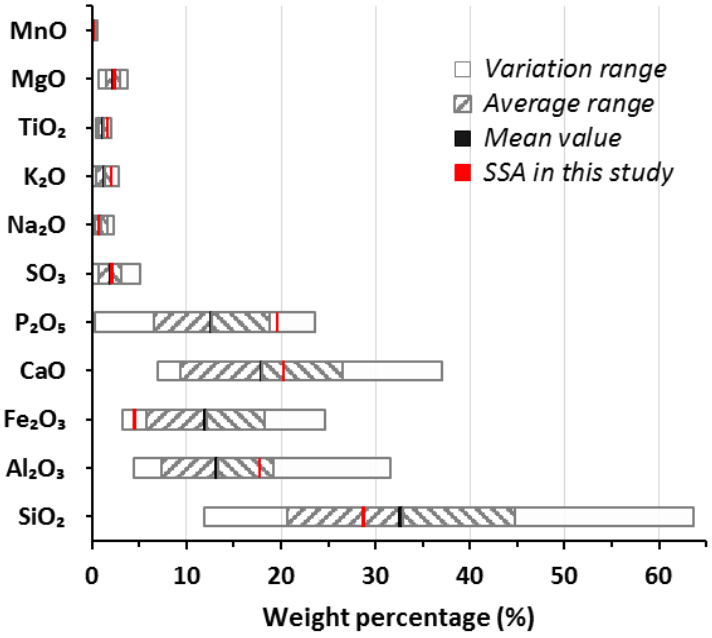

Fig. 2. Variability of the chemical composition of the studied SSA (in red) compared to other SSA found in the literature.

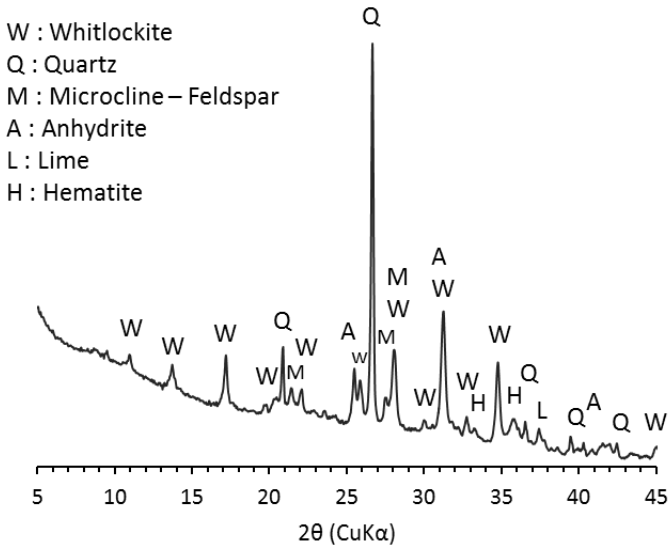

Fig. 3. X-ray diffraction pattern of the investigated SSA, with the identification of the main phases.

3.2 Reactivity of SSA

The hydraulic and pozzolanic properties of SSA were evaluated using isothermal calorimetry and XRD analyses. The mixtures with distilled water and KOH solution (0.1 mol/L, i.e. pH = 13) showed no significant heat release or hardening, thus it can be concluded that SSA has no self-cementitious or hydraulic properties. These observations concur with the results of former studies, showing no phase changes except the dissolution of gypsum [3,22]. On the other hand, however, the heat flow curves of the SSA-CH mixtures displayed a distinguishable peak about two hours following the initial contact with water. Fig. 4 illustrates the heat flow evolution per g of solid, as measured by isothermal calorimetry. The cumulative heat values after six days of reaction were 96 and 56 J per g of solid for the 50SSA50CH and 25SSA75CH mixtures, respectively. Although this is an indication that the SSA reacts in presence of calcium, further investigations are required to assume the pozzolanic activity of SSA. In this respect, XRD analyses were simultaneously employed to follow the phase change in the CH-SSA within the first hours of reaction.

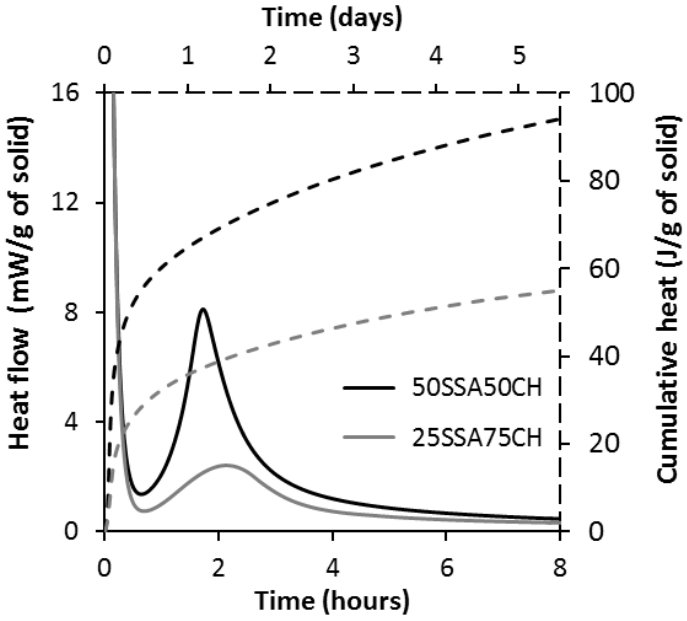

Fig. 4. Heat flow calorimetry results of the SSA-CH systems at w/s ratio of 1. Solid lines represent the heat flow over the first hours while the dashed lines show the evolution of the cumulative heat during the first days. The results are normalised per g of solid.

In order to predict the phases that might form in SSA-CH mixtures, the fraction of elements mobilized in the solution upon the dissolution of SSA was calculated. For this purpose, SSA was placed in two mediums: distilled water (neutral pH) and KOH solution (pH = 13). The solutions were sealed for a month (to avoid contamination) and the elements in the solution were quantified using ICP-AES. The results are reported in Table 4. On the other hand, given the weak solubility of the crystalline phases composing SSA (e.g. quartz, whitlockite, feldspar), it is expected that the majority of element governing its reaction are provided by the glassy phase (≈48 wt.%). Therefore, the average composition of the SSA amorphous phase was calculated by subtracting the contribution of the crystalized phases from the bulk composition determined by X-ray fluorescence. As shown in Table 4, the SSA amorphous phase is mainly composed of alumina (≈17.3 wt.%) and silicon (≈11.9 wt.%). These observations are in line with the ICP-AES results, showing that the aluminium and, to some extent phosphates, are the most soluble phase while the dissolution of other elements is negligible. Therefore, combining these information, the calcium aluminates hydrates (probably AFt, hydrogarnet or AFm) are the most likely phases to form in presence of portlandite. Furthermore, with the majority of P_2O_5 being inert in the structure of the whitlockite (13.26 out of 19.5 wt.%), only 0.644 wt.% has dissolved in KOH solution. Consequently, it is realistic to assume that the phosphate will not heavily impact the products of hydration.

Table 4. Composition of the glassy phase of SSA.

	Amorphous phase composition (wt.%)	***Dissolved amount in distilled water (wt.%)***	***Dissolved amount in KOH solution (wt.%)***
pH		***9.7***	***12.1***

SiO_2	11.93	0.003	0.003
CaO	4.95 + 1.28*	0.790	> 0.001
Al_2O_3	17.34	0.025	1.580
Fe_2O_3	3.97	> 0.001	> 0.001
Na_2O	0.62	0.031	> 0.001
K_2O	1.21	0.080	0.169
P_2O_5	6.84	0.002	0.644
SO_3	0.24 + 1.82*	1.242	0.746
MgO	1.39	0.007	> 0.001

*Anhydrite

Fig. 5 depicts the X-ray diffractograms of the 50SSA50CH mixture at different ages of hydration. After two hours of hydration, the XRD patterns revealed the apparition of the characteristic peaks of monocarboaluminates ($C_4A\bar{C}H_{11}$) and ettringite, respectively at 7.6 Å and 9.7 Å. The amounts of monocarboaluminates and ettringite increased while the portlandite peaks intensity decreased within the first hours of hydration. These results are in agreement with the fact that aluminium is the main element being introduced to the system upon the dissolution of SSA. At 7 days, besides the formation of gypsum due to the hydration of anhydrite, a second peak appeared around 8.2 Å. This peak was attributed to the formation of hemicarboaluminates ($C_4A\bar{C}_{0.5}H_{12}$). The increase of its intensity with reaction time coincides with the decrease in the portlandite content. Similar observations were reported by [57,58], showing that the excess of portlandite in a mixture containing monocarboaluminates results in the formation of hemicarboaluminates. Furthermore, the diffraction patterns showed no sign of ettringite after 28 days although the presence of monocarboaluminates are reported to stabilise the AFt phase [59]. Instead the remaining hydration products were hemi- and monocarboaluminates, and gypsum.

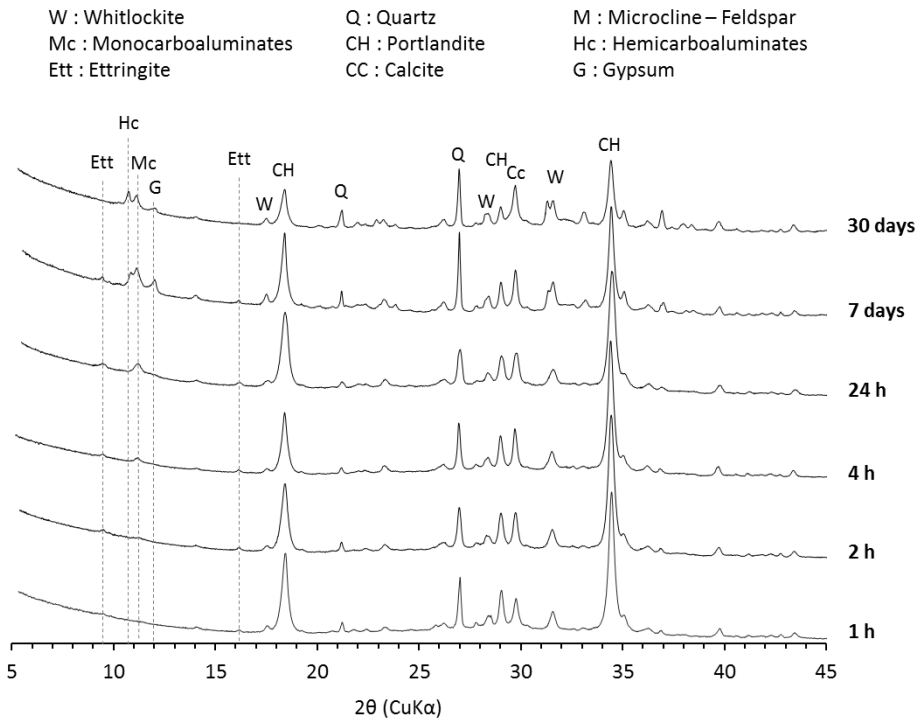

Fig. 5. XRD patterns of 50SSA50CH system at different hydration times.

4 Influence of SSA on cement hydration

4.1 Compressive strength and electrical resistivity

The influence of sewage sludge ashes on compressive strength (*f'c*) and electrical resistivity was investigated by comparing the behaviour of mortars containing 20% SSA (20SSA) to a control (OPC) and a 20% FA-blended (20FA) mortars. Fig. 6 presents the measured compressive strength and resistivity of the produced mortars at 1, 2, 7, 28, 56, and 182 days of hydration. The compressive strength results of 20SSA showed a steep increase in the first days of hydration, that exceed both control and 20FA mortars. However, after 28 days of hydration, the strength of the control and 20FA surpassed the mortar containing SSA. On the other hand, the blended systems (20FA and 20SSA) show a higher resistivity than the control (respectively 5.5, 11.3 and 30.9 KΩ.cm for control, 20SSA and 20FA at 182 days). This is more likely related to a more refinement of the microstructure and pore distributions.

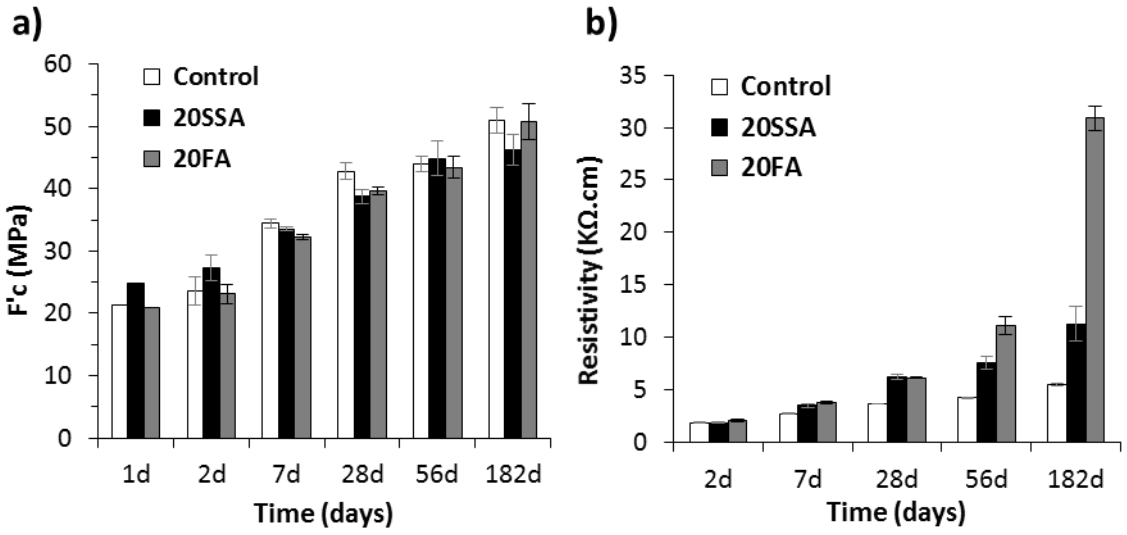

Fig. 6. a) Compressive strength, f'c (MPa) and b) Electrical resistivity (kΩ.cm) of OPC, 20SSA and 20FA mortars.

4.2 Hydration kinetics and setting time

The heat evolution curves of the control and SSA-modified pastes, normalised to the amount of cement, are displayed in Fig. 7. The pastes containing SSA can be clearly discerned as they show a second peak (around 20–30 hours of hydration) as opposed to the control (OPC) heat curve where only the main peak of hydration is observed. Steeper heat liberation is observed on the second peak in the pastes with higher SSA content, and thus the apparition of the second peak could be explained by the reactivity of the SSA replacements. Furthermore, an extension of the acceleration period and a shift of the first heat peak maximum towards later ages has been observed on the heat curves when SSA is used. These results are consistent with the Vicat needle measurements (NF EN 196-3), showing the retardation effect of SSA. As shown in Fig. 8, increasing SSA content led to a further delay in both the initial and final setting times compared to a control mortar. For a 30% SSA replacement, the initial setting was obtained 1:40 after the control while the setting time was increased by 2 hours, so a total delay of 3:40. Similar observation has been reported by previous studies [3,43,60].

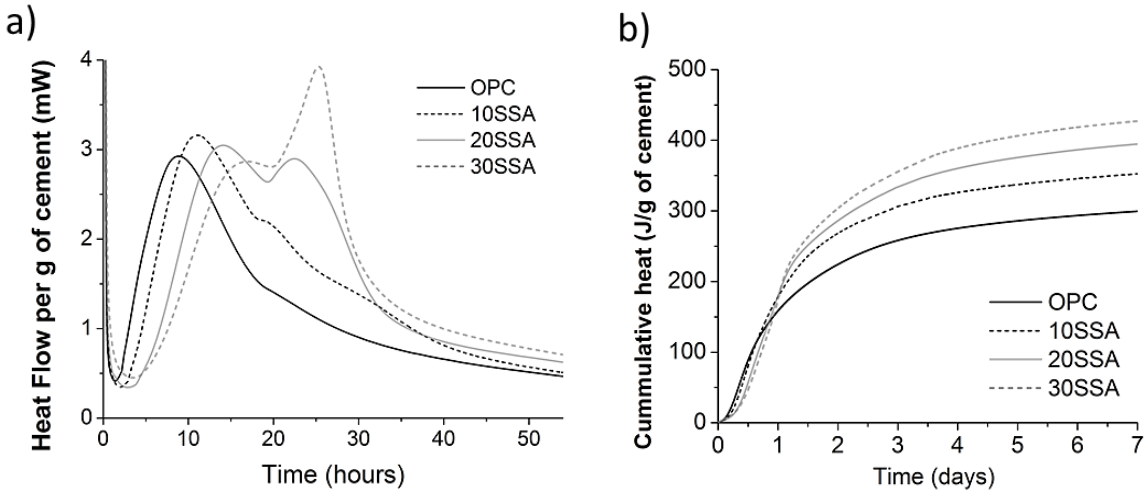

Fig. 7. Influence of the SSA substitution rate on the heat liberation: a) Heat flow and b) cumulative heat per g of cement

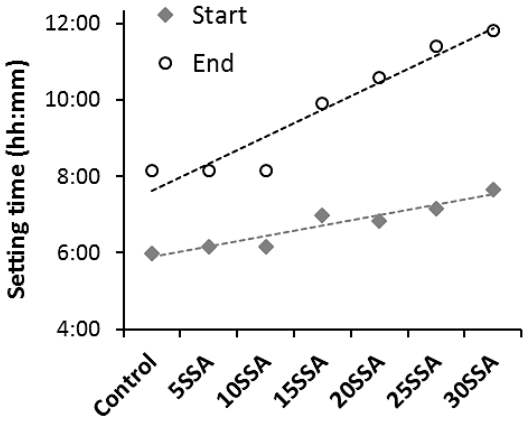

Fig. 8. Influence of SSA substitution rate on the setting time

The delay in the cement hydration and setting time when SSA is used could be explained by the presence of the orthophosphate ions (PO_4^{3-}), which are known to inhibit the growth of crystals [61]. In fact, several authors have reported the retarding effect of the orthophosphate on the cement hydration [62–64]. In the same manner that gypsum (particularly sulphates) slows down the reaction of C_3A, the adsorption of phosphates ions on the reactive sites of C_3S hinders its dissolution rate [61]. Furthermore, Benard et al. [65] have shown a discontinuity of the retarding effect above a pessimum phosphate concentration of 0.2 mol/L. This change of behaviour have been attributed to the precipitation of hydroxyapatite, due to the saturation of the silicate dissolution sites. However, the solubility of P_2O_5 in SSA (see Table 4) is rather low, and thus the adsorption of phosphates ions on the different phases constituting the cementitious matrix is more likely than the formation of calcium phosphates compounds.

4.3 Clinker phases evolution

The degree of hydration of clinker as function of time is given in Fig. 9, as measured by XRD-Rietveld refinement. Similarly to the calorimetry observations, the inclusion of SSA seems to delay the hydration of cement at early age. For instance, only 57% of clinker has reacted in the 20SSA system whereas the cement dissolution was faster in the neat OPC system with over than 65% having reacted within the first day of hydration. Eventually, the cement hydration in SSA blended systems reaches similar degree of reaction as the control. Moreover, the influence of SSA on the individual clinker phases' hydration is summarized in Table 5. Upon the addition of SSA, the hydration of alite was slowed down, notably in the first days of hydration. The hydration of C_3A, on the other hand, seems also to be delayed but only marginally. In contrast, no discernible effect were observed on the belite and ferrite rates of hydration. The effect of SSA on the hydration of alite is probably related to the adsorption of the orthophosphates ions on its surface, as explained above.

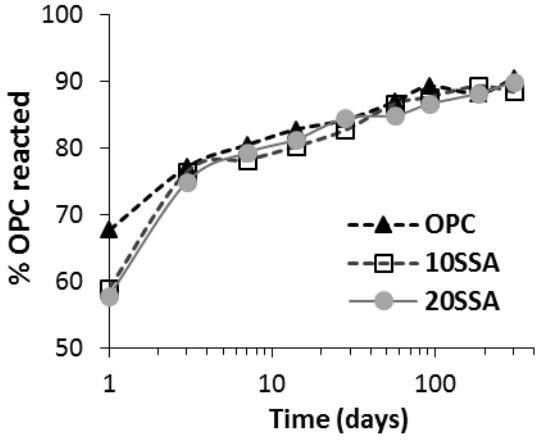

Fig. 9. Degree of the reaction of cement as measured by XRD-Rietveld refinement

Table 5. Evolution of clinker phases as a function of hydration time. The value are normalised to the cement content (g per g of cement).

	Time (days)	C_3S	C_2S	C_3A	C_4AF
OPC	1	12.5	7.8	1.1	3.3
	3	6.4	7.4	0.8	2.8
	7	4.7	6.7	0.8	2.6
	14	3.6	6.5	0.6	2.4
	28	3.5	6.0	0.4	2.1
	56	2.4	4.9	0.5	2.2
	91	1.9	4.0	0.5	1.8
	182	2.2	4.1	0.5	2.1
	300	1.2	3.7	0.5	2.0
10SSA	1	19.1	6.6	2.0	3.6
	3	8.2	5.9	1.3	2.6
	7	7.3	5.5	1.2	2.6
	14	6.3	5.6	0.8	2.3

	28	5.8	4.6	0.8	2.0
	56	3.8	4.0	0.7	1.7
	91	3.2	3.8	0.6	1.9
	182	2.4	3.2	0.7	1.8
	300	2.7	3.6	0.7	1.7
20SSA	1	19.8	6.9	2.1	3.5
	3	9.1	6.4	1.1	2.6
	7	6.9	5.8	0.9	2.2
	14	6.0	5.7	0.6	2.0
	28	4.8	4.7	0.5	1.8
	56	4.8	4.3	0.8	1.7
	91	3.9	4.1	0.5	1.7
	182	3.0	3.9	0.4	1.7
	300	2.5	3.3	0.3	1.5

4.4 Portlandite consumption

The replacement of cement by SSA leads to the formation of lesser amount of portlandite, which is even lower when normalised back to the mass of cement. Fig. 10(a) shows the evolution of the portlandite content normalised to cement content, as measured by the tangent method from the DTG curves (derivative of the thermogravimetric curve) [35]. Furthermore, the consumption of portlandite per g of SSA, calculated by subtracting the expected amount of CH produced by each g neat OPC, is given in Fig. 10(b). The results show that the increase of SSA substitution rate results in the decrease of portlandite content (0.13 vs. 0.10 g per g of cement for 10SSA vs. 20SSA at 300 days). However, the reactivity of SSA seems to be higher in the 10SSA with 0.42 g of CH consumed by g of SSA compared to 0.29 g of CH per g of SSA in the 20SSA mix. Additionally, the majority of CH is consumed within the first days while no significant change occurs at later age (56 days and onwards), particularly for 20SSA mix. This might be related to the type and/or the amounts of the hydrates which will be discussed subsequently. It is worth mentioning the amount of CH measured by XRD-Rietveld are in line with the TGA results (+/- 1 wt.%).

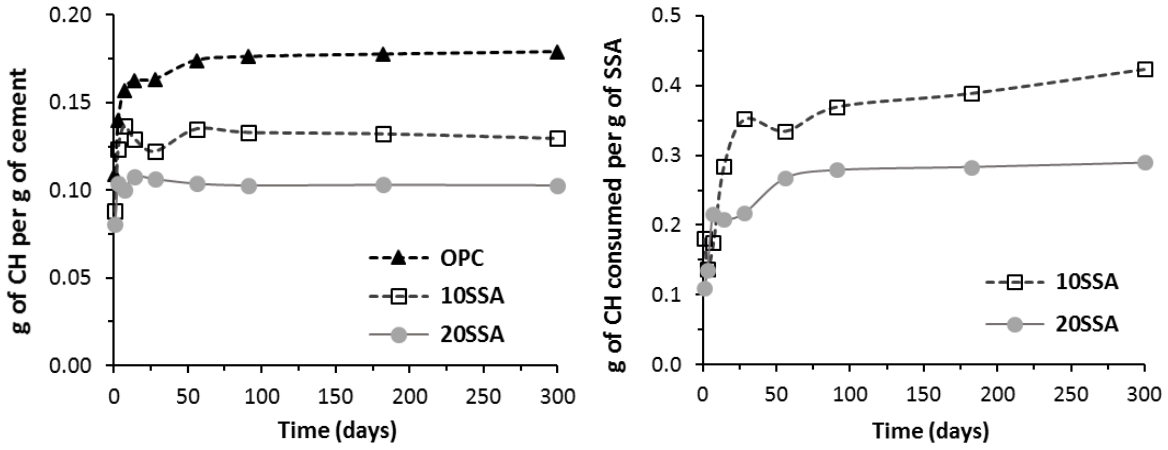

Fig. 10. : a) Evolution of the amount of calcium hydroxide (CH) per g of cement and b) Evolution of CH consumed by the reaction in SSA in blended systems (g per g)

4.5 AFm and AFt phases

Fig. 11 presents normalised ^{27}Al MAS NMR spectra of the OPC, 10SSA and 20SSA systems hydrated for 7, 28, and 300 days. The spectra yield three distinguishable resonances between 100-50 ppm over the spectral range for the Al(IV) (i.e. Al in tetrahedral coordination). The observed peaks with centers at ≈ 81 ppm and ≈ 70 ppm are respectively assigned to Al substituting for Si in the alite/betite and the C-S-H phase [59,66,67]. On the other hand, the broadened signal with low intensity at about 58 ppm, appearing only in the blended systems, is attributed to the contribution of SSA. It is worth mentioning that the Al incorporation in C-S-H increases with the SSA inclusion and with reaction time. Moreover, the SSA displays another peak around 39 ppm, which intensity decreases for higher curing time. At lower frequencies, the chemical shift region for Al in octahedral coordination (from -10 to 20 ppm) shows three peaks which are attributed to the presence of (i) ettringite at ≈ 13.5 ppm, (ii) AFm phases at ≈ 9.8 ppm and finally (iii) unknown "Third Aluminate Hydrate" at about 5 ppm [68–70]. Even though the ^{27}Al MAS NMR spectra show clearly an increase in the AFm content in the SSA-blended systems, the fine distinction between the different AFm phases is not possible [59,66,71]. In fact, the monosulfoaluminates, hemi- and monocarboaluminates have very similar chemical shift and quadrupole coupling parameters, and thus their contribution cannot be deconvoluted using the ^{27}Al NMR spectra alone. Therefore, the occurrence of the AFm phases in SSA-modified pastes was further investigated using XRD.

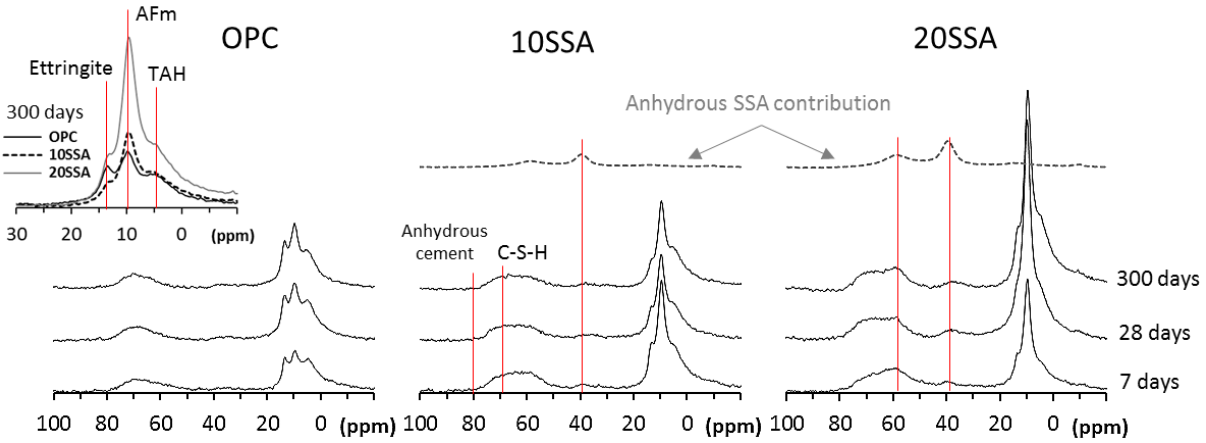

Fig. 11. ^{27}Al MAS NMR spectra of hydrated OPC, 10SSA and 20SSA for 7, 28 and 300 days. In the upper left corner, ^{27}Al MAS NMR spectra over a (-10)–30 ppm range, used to compare the ettringite and AFm phases contents in the 300-days hydrated systems

Fig. 12 displays details of the XRD diffractograms of hydrated OPC and 20SSA systems for 1, 7, 28 and 300 days. The patterns are compared over an angular range of 8-12° 2θ (CuKα), which allows the distinction between the various AFm phases. Overall, the identified crystalline phases are ettringite and monocarboaluminates, which are common to both OPC and 20SSA. Moreover, a low intensity reflection of the hemicarboaluminates is detected in the 300 days hydrated 20SSA sample. Quantitatively, the amounts of ettringite and monocarboaluminates in the blended system are higher than the OPC systems after 300 days of hydration (respectively 10.9 and 11.0 vs. 8.2 and 2.8 g per g of cement). As aforementioned, this could be explained by the aluminium content in the SSA and the initial presence of limestone in cement. Indeed, the ettringite, formed during the reaction between C_3A and calcium sulphates, might convert to monosulfoaluminates ($C_4A\bar{S}H_{12}$) upon the depletion of free sulphate and/or the continuing supply of Al to the system. Furthermore, in presence of calcite, the SO_4^{2-} in the interlayer of monosulfates are substituted by CO_3^{2}, which leads to the formation of calcium carboaluminates hydrates [57,59,72,73]. Additionally, these observations are in line with the ^{27}Al NMR results, showing the decrease of SSA signal at about 39 ppm (i.e. dissolution of aluminium in SSA).

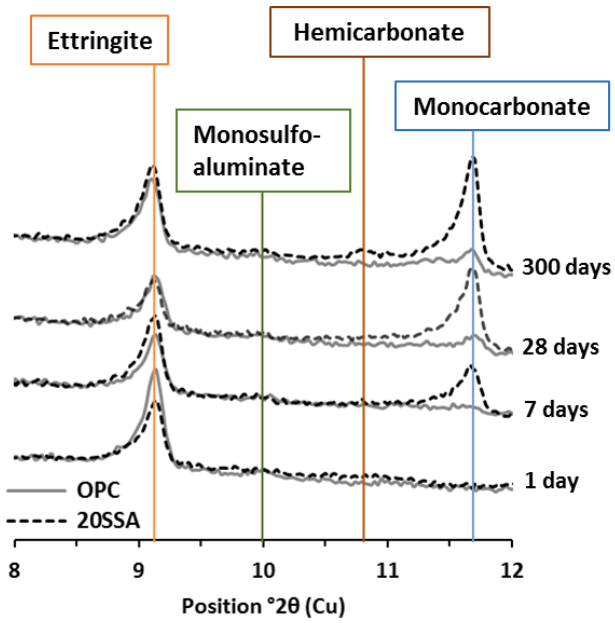

Fig. 12. Diffraction patterns of hydrated Portland cement (OPC, full grey line) and modified cement with 20 wt.% sewage sludge ash (20SSA, dotted line) at 1, 7, 28 and 300 days of hydration. The diffractograms are compared in an angular window of 8–12° 2θ (CuKα), which allows the identification of AFm and AFt phases.

4.6 Chemically bound water content

The non-evaporable water content is typically used to assess the degree of reaction of the plain Portland cements [35,74,75]. However, the interpretation of the bound water becomes more complicated when the SCMs are incorporated in the pastes. This comes down to the fact that SCMs and clinker phases reaction occurs simultaneously, which makes it a difficult task to separate the contribution of each material in the measured bound water. In this study, the non-evaporable water content of SSA-modified pastes was contrasted to a control in order to highlight the differences in hydration process between the binders. Therefore, the bound water was measured by thermogravimetric (mass loss at 1000 °C without the carbonates contributions) and the results are normalised to cement content of the systems. To accurately determine the amount of bound water, the sample was prepared as follows: the hardened pastes were ground then immersed in isopropanol for 15 min to replace the unbound water in the capillary pores, the isopropanol was then removed by diethyl ether and the powders were subsequently subject to short vacuum drying to remove the residual solvents.

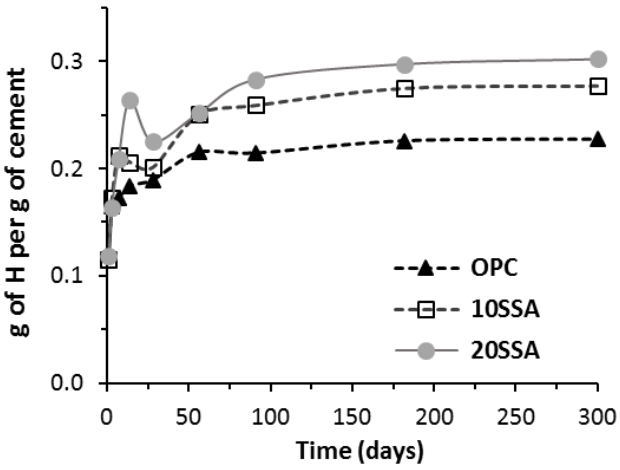

Fig. 13. Evolution of bound water content per g of cement as a function of time.

Overall, the SSA blends have a slightly higher amount of bound water per g of binder. However, the differences are more significant when the non-evaporable is reported to the cement content, as shown in Fig. 13. It could be explained by the different type of product formed during the hydration (e.g. monocarboaluminates) as shown by XRD/Rietveld results. Furthermore, the SSA modified systems shows a loss in the bound water between 7 and 56 days. More interestingly, this loss coincides with the dissolution of ettringite and the formation of the monocarboaluminates phase, as shown in Fig. 14. The ettringite content decrease is probably related to the depletion of alumina during the formation of monocarboaluminates, which is considered as the most stable phase. However, the continuous supply of Al through the dissolution of SSA amorphous phase resulted in the precipitation of ettringite after 56 days, and thus the increase of bound water.

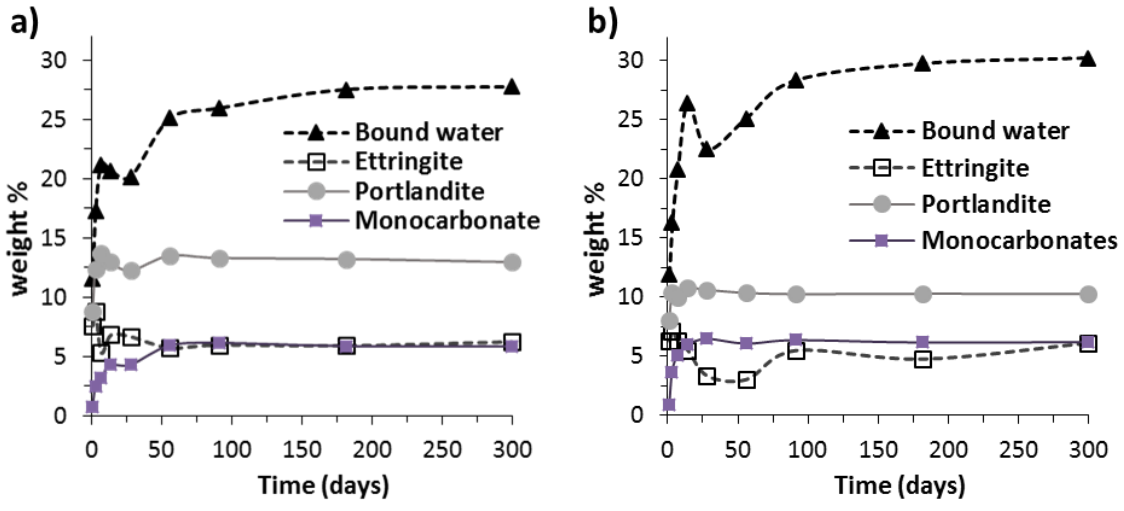

Fig. 14. Evolution of the main phase as a function of time in the systems a) 10SSA and b) 20SSA. The ettringite and monocarboaluminates are expressed in wt.% in hydrated sample, while the bound water and portlandite content are normalized to the cement content.

5. DISCUSSION

The partial replacement of cement by SSA results in a delay in the setting time of the cement paste (around 2 hours with 20 wt.% SSA). This could be explained by the slowdown of the C_3S hydration due to the adsorption of orthophosphate ions on the dissolution site of this phase. This assumption is confirmed by the XRD-Rietveld results, showing a retardation in the alite degree of reaction, particularly within the first days of hydration. Nonetheless, the overall hydration of cement seems unaffected at later age. Furthermore, the use of SSA leads to the apparition of a second peak on the heat flow curve. This heat liberation has been attributed to the formation of calcium aluminate hydrates due the continuous supply of aluminium to the system upon the dissolution of the amorphous phase of SSA. On the other hand, the majority phosphates in SSA are in form of whitlockite, a calcium phosphate mineral with a weak solubility [76], whereas the remaining amount (about 6.84 wt.%) is included in the amorphous phase. However, the dissolution of the amorphous P_2O_5 is found to be very low, therefore the formation of hydroxyapatite (or other calcium phosphate compounds) is deemed unlikely.

The compressive strength of SSA cements surpass that of neat OPC at early age. This is because of the change in the phase assemblage, which is governed by the bulk composition of the system [59,77,78]. Indeed, the SSA contains high amount of reactive aluminium, and thus the formation of AFt and AFm phases is promoted. As confirmed by the experimental results, the ettringite and AFm phases (notably monocarboaluminates) content in SSA blends is higher than in the neat OPC system. Therefore, these modifications in the hydration products lead to changes in the total volume of solid, and thus the mechanical and durability properties. These observations are in line with the thermodynamic simulation (see Fig. 15), showing the formation of ettringite and monocarbonates, while the formation hemicarbonates instead of monocarbonates is calculated for higher replacement level. It should be noted that simulated phase assemblage here is based on the assumption that 90% of the cement has reacted whereas 50% of the amorphous phase of SSA has dissolved. Overall, the thermodynamic modelling agrees well with the experimental observations. It is also worth mentioning that the XRD patterns have revealed the simultaneous occurrence of AFt, hemi-, and monocarboaluminates in the 20SSA system at 300 days (see Fig. 12) while the model did not predict the coexistence of these phases. This could be explained by the amount of SSA assumed to dissolve (i.e. alumina introduced to the system) and/or the amount of calcite available to react (i.e. the increase of CO_2 promote the formation of hemicarboaluminates over the monocarbonates).

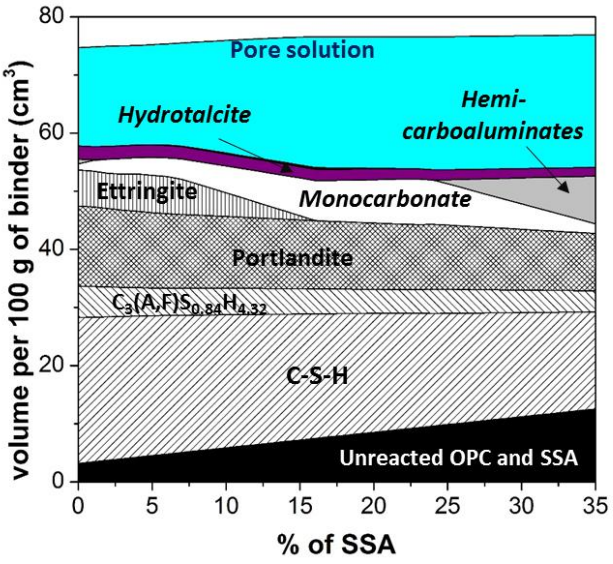

Fig. 15. Thermodynamic modelling of the phase assemblage as a function of the SSA addition. Only 50% of the SSA amorphous phase is assumed to react.

6. Conclusion

In this work, the influence of the partial replacement of cement by SSA on its hydration and the phase assemblage of the cementitious matrix is investigated. The following conclusions can be drawn according to the findings of this study:

- As evidenced by the calorimetry results, the inclusions of SSA delays to hydration of the cement, particularly the alite, due to the presence of orthophosphate ions.
- Even though the chemical and mineralogical composition of SSA appears to fluctuate significantly, only the amorphous phase seems to participate in the reaction.
- Being the most soluble element, aluminium is found to affect the amount of formed AFt and AFm phases, notably the monocarboaluminates. These experimental observations have been confirmed by thermodynamic modelling.
- The enhancement of the macro-scale properties of mortars can be explained by the changes in the solid volume, as a result of the formation of different hydrates.
- The fraction of phosphates mobilised into solution is considered insufficient to form calcium phosphates compounds.

Considering the reaction products and the macro-scale results, the use of SSA as a cement component is feasible. However, further studies are still require to extend the boundaries of knowledge concerning the long-term and durability aspects of SSA blended cements.

REFERENCES

[1] D. Fytili, A. Zabaniotou, Utilization of sewage sludge in EU application of old and new methods—A review, Renew. Sustain. Energy Rev. 12 (2008) 116–140. doi:10.1016/J.RSER.2006.05.014.

[2] C.J. Lynn, R.K. Dhir, G.S. Ghataora, R.P. West, Sewage sludge ash characteristics and potential for use in concrete, Constr. Build. Mater. 98 (2015) 767–779. doi:10.1016/j.conbuildmat.2015.08.122.

[3] M. Cyr, M. Coutand, P. Clastres, Technological and environmental behavior of sewage sludge ash (SSA) in cement-based materials, Cem. Concr. Res. 37 (2007) 1278–1289. doi:10.1016/j.cemconres.2007.04.003.

[4] Y.J. Park, S.O. Moon, J. Heo, Crystalline phase control of glass ceramics obtained from sewage sludge fly ash, Ceram. Int. (2003). doi:10.1016/S0272-8842(02)00109-8.

[5] S. Suzuki, M. Tanaka, T. Kaneko, Glass-ceramic from sewage sludge ash, J. Mater. Sci. (1997). doi:10.1023/A:1018584202392.

[6] Y.Q. Gan, Y.X. Wang, Y.L. Guo, Preparation of ceramic tile from sewage sludge pyrolysis ash, Proc. Int. Symp. Water Resour. Urban Environ. (2003).

[7] M. Kosior-Kazberuk, Application of SSA as partial replacement of aggregate in concrete, Polish J. Environ. Stud. 20 (2011) 365–370.

[8] I.-J. Chiou, K.-S. Wang, C.-H. Chen, Y.-T. Lin, Lightweight aggregate made from sewage sludge and incinerated ash, Waste Manag. 26 (2006) 1453–1461. doi:10.1016/j.wasman.2005.11.024.

[9] M.M. AI-Sharif, M.F. Attom, A geoenvironmental application of burned wastewater sludge ash in soil stabilization, Environ. Earth Sci. 71 (2014) 2453–2463. doi:10.1007/s12665-013-2645-z.

[10] D.-F. Lin, C.-H. Weng, Use of Sewage Sludge Ash as Brick Material, J. Environ. Eng. (2002). doi:10.1061/(asce)0733-9372(2001)127:10(922).

[11] S. Donatello, C.R. Cheeseman, Recycling and recovery routes for incinerated sewage sludge ash (ISSA): A review, Waste Manag. (2013). doi:10.1016/j.wasman.2013.05.024.

[12] M. Anderson, R.G. Skerratt, J.P. Thomas, S.D. Clay, Case study involving using fluidised bed incinerator sludge ash as a partial clay substitute in brick manufacture, Water Sci. Technol. (1996). doi:10.1016/0273-1223(96)00618-X.

[13] E.J. Trauner, Sludge Ash Bricks Fired to above and below Ash-Vitrifying Temperature, J. Environ. Eng. (2006). doi:10.1061/(asce)0733-9372(1993)119:3(506).

[14] C.J. Lynn, R.K. Dhir, G.S. Ghataora, Sewage sludge ash characteristics and potential for use in bricks, tiles and glass ceramics, Water Sci. Technol. (2016). doi:10.2166/wst.2016.040.

[15] M. Anderson, R.G. Skerratt, Variability study of incinerated sewage sludge ash in relation to future use in ceramic brick manufacture, Br. Ceram. Trans. 102 (2003) 109–113. doi:10.1179/096797803225001614.

[16] D.F. Lin, W.C. Chang, C. Yuan, H.L. Luo, Production and characterization of glazed tiles containing incinerated sewage sludge, Waste Manag. (2008). doi:10.1016/j.wasman.2007.01.018.

[17] D.F. Lin, H.L. Luo, Y.N. Sheen, Glazed tiles manufactured from incinerated sewage sludge ash and clay, J. Air Waste Manag. Assoc. (2005). doi:10.1080/10473289.2005.10464614.

[18] J. Monzó, J. Payá, M.. Borrachero, E. Peris-Mora, Mechanical behavior of mortars containing sewage sludge ash (SSA) and Portland cements with different tricalcium aluminate content,

Cem. Concr. Res. 29 (1999) 87–94. doi:10.1016/S0008-8846(98)00177-X.

[19] Z. Chen, C.S. Poon, Comparative studies on the effects of sewage sludge ash and fly ash on cement hydration and properties of cement mortars, Constr. Build. Mater. 154 (2017) 791–803. doi:10.1016/J.CONBUILDMAT.2017.08.003.

[20] F. Baeza, J. Payá, O. Galao, J.M. Saval, P. Garcés, Blending of industrial waste from different sources as partial substitution of Portland cement in pastes and mortars, Constr. Build. Mater. 66 (2014) 645–653. doi:10.1016/J.CONBUILDMAT.2014.05.089.

[21] P. Garcés, M. Pérez Carrión, E. García-Alcocel, J. Payá, J. Monzó, M. V. Borrachero, Mechanical and physical properties of cement blended with sewage sludge ash, Waste Manag. 28 (2008) 2495–2502. doi:10.1016/j.wasman.2008.02.019.

[22] F. Frohard, Durability of green concretes : impact of alternative cementitious materials on the corrosion of steel in reinforced concrete, PhD thesis, Paris-Est University (2014).

[23] Y. fan Zhou, J. shan Li, J. xin Lu, C. Cheeseman, C.S. Poon, Sewage sludge ash: A comparative evaluation with fly ash for potential use as lime-pozzolan binders, Constr. Build. Mater. 242 (2020) 118160. doi:10.1016/j.conbuildmat.2020.118160.

[24] Y. fan Zhou, J. shan Li, J. xin Lu, C. Cheeseman, C.S. Poon, Recycling incinerated sewage sludge ash (ISSA) as a cementitious binder by lime activation, J. Clean. Prod. 244 (2020) 118856. doi:10.1016/j.jclepro.2019.118856.

[25] P. de Azevedo Basto, H. Savastano Junior, A.A. de Melo Neto, Characterization and pozzolanic properties of sewage sludge ashes (SSA) by electrical conductivity, Cem. Concr. Compos. 104 (2019) 103410. doi:10.1016/j.cemconcomp.2019.103410.

[26] T.D. Dyer, J.E. Halliday, R.K. Dhir, J.E. Halliday, R.K. Dhir, Hydration Chemistry of Sewage Sludge Ash Used as a Cement Component, 2011. doi:10.1061/(ASCE)MT.1943-5533.0000221.

[27] P.-Y. Mahieux, J.-E. Aubert, M. Cyr, M. Coutand, B. Husson, Quantitative mineralogical composition of complex mineral wastes – Contribution of the Rietveld method, Waste Manag. 30 (2010) 378–388. doi:10.1016/J.WASMAN.2009.10.023.

[28] M. Willems, B. Pedersen, S.S. Jørgensen, Composition and Reactivity of Ash from Sewage Sludge, Ambio. 5 (1976) 32–35. doi:10.2307/4312161.

[29] S. Nanzer, A. Oberson, T. Huthwelker, U. Eggenberger, E. Frossard, The Molecular Environment of Phosphorus in Sewage Sludge Ash: Implications for Bioavailability, J. Environ. Qual. 43 (2014) 1050. doi:10.2134/jeq2013.05.0202.

[30] A. Ohbuchi, J. Sakamoto, M. Kitano, T. Nakamura, X-ray fluorescence analysis of sludge ash from sewage disposal plant, X-Ray Spectrom. 37 (2008) 544–550. doi:10.1002/xrs.1085.

[31] C. Adam, B. Peplinski, M. Michaelis, G. Kley, F.-G. Simon, Thermochemical treatment of sewage sludge ashes for phosphorus recovery, Waste Manag. 29 (2009) 1122–1128. doi:10.1016/j.wasman.2008.09.011.

[32] ASTM C150 / C150M-18, Standard Specification for Portland Cement, 2018. doi:10.1520/C0150_C0150M-18.

[33] M. Saillio, L. Andrade, M. Mejdi, T. Chaussadent, A. Tagnit-Hamou, Properties of cementitious materials with sewage sludge ashes, *Proceedings of the International Conference on Sustainable Materials, Systems and Structures (SMSS2019) : New Generation of Construction Materials*, ROVINJ, Croatia. (2019) 156-163

[34] M. Mejdi, W. Wilson, M. Saillio, T. Chaussadent, L. Divet, A. Tagnit-Hamou, Investigating the pozzolanic reaction of post-consumption glass powder and the role of portlandite in the formation of sodium-rich C-S-H, Cem. Concr. Res. 123 (2019) 105790.

542 doi:10.1016/j.cemconres.2019.105790.

543 [35] K. Scrivener, R. Snellings, B. Lothenbach, A Practical Guide to Microstructural Analysis of
544 Cementitious Materials, 2016. doi:10.7693/wl20150205.

545 [36] M. Mejdi, W. Wilson, M. Saillio, T. Chaussadent, L. Divet, A. Tagnit-Hamou, Quantifying glass
546 powder reaction in blended-cement pastes with the Rietveld-PONKCS method, Cem. Concr.
547 Res. 130 (2020) 105999.

548 [37] L.C. Morais, J. Dweck, E.M. Gonçalves, P.M. Büchler, An experimental study of sewage sludge
549 incineration, Environ. Technol. 27 (2006) 1047–1051. doi:10.1080/09593332708618718.

550 [38] J.-H. Tay, K.-Y. Show, Utilization of municipal wastewater sludge as building and construction
551 materials, Resour. Conserv. Recycl. 6 (1992) 191–204. doi:10.1016/0921-3449(92)90030-6.

552 [39] K.-L. Lin, C.-Y. Lin, Hydration Properties of Eco-Cement Pastes from Waste Sludge Ash Clinkers,
553 J. Air Waste Manag. Assoc. J. J. Air Waste Manag. Assoc. 5412 (2004) 1096–2247.
554 doi:10.1080/10473289.2004.10471011.

555 [40] C. Schaum, P. Cornel, N. Jardin, Phosphorus recovery from sewage sludge ash–a wet chemical
556 approach, Proceeding IWA Conf. …. (2007) 583–590.
557 http://www.sswm.info/sites/default/files/reference_attachments/SCHAUM et al ny Phosphorus
558 Recovery from Sewage Sludge Ash.pdf.

559 [41] F.C. Chang, J.D. Lin, C.C. Tsai, K.S. Wang, Study on cement mortar and concrete made with
560 sewage sludge ash, Water Sci. Technol. 62 (2010) 1689–1693. doi:10.2166/wst.2010.459.

561 [42] S. Donatello, M. Tyrer, C.R. Cheeseman, EU landfill waste acceptance criteria and EU Hazardous
562 Waste Directive compliance testing of incinerated sewage sludge ash, Waste Manag. 30 (2010)
563 63–71. doi:10.1016/j.wasman.2009.09.028.

564 [43] T.D. Dyer, J.E. Halliday, R.K. Dhir, Hydration Chemistry of Sewage Sludge Ash Used as a Cement
565 Component, J. Mater. Civ. Eng. 23 (2011) 648–655. doi:10.1061/(ASCE)MT.1943-5533.0000221.

566 [44] A. Magdziarz, M. Wilk, M. Gajek, D. Nowak-Woźny, A. Kopia, I. Kalemba-Rec, J.A. Koziński,
567 Properties of ash generated during sewage sludge combustion: A multifaceted analysis, Energy.
568 113 (2016) 85–94. doi:10.1016/j.energy.2016.07.029.

569 [45] J.E. Halliday, M.R. Jones, T.D. Dyer, R.K. Dhir, Potential use of UK sewage sludge ash in cement-
570 based concrete, Proc. Inst. Civ. Eng. - Waste Resour. Manag. 165 (2012) 57–66.
571 doi:10.1680/warm.2012.165.2.57.

572 [46] M. Franz, Phosphate fertilizer from sewage sludge ash (SSA), Waste Manag. 28 (2008) 1809–
573 1818. doi:10.1016/j.wasman.2007.08.011.

574 [47] K.L. Lin, W.C. Chang, D.F. Lin, H.L. Luo, M.C. Tsai, Effects of nano-SiO2 and different ash particle
575 sizes on sludge ash–cement mortar, J. Environ. Manage. 88 (2008) 708–714.
576 doi:10.1016/j.jenvman.2007.03.036.

577 [48] A. Zidol, Durabilité en milieux agressifs des bétons incorporant la poudre de verre, PhD thesis,
578 Université de Sherbrooke (2014).

579 [49] D. Michaud, Bilan 2015 de la gestion des matières résiduelles au Québec Mot du président-
580 directeur général, (n.d.). https://www.recyc-
581 quebec.gouv.qc.ca/sites/default/files/documents/bilan-gmr-2015.pdf (accessed May 11, 2018).

582 [50] D. Vouk, D. Nakic, M. Serdar, S. Donatello, C.R. Cheeseman, Evaluation of using sewage sludge
583 ash in the cement industry: Case study of Zagreb, Croatia, in: IWA Spec. Conf. Sludge Manag.
584 Sludgetech, 2017.

585 [51] P. He, C.S. Poon, D.C.W. Tsang, Using incinerated sewage sludge ash to improve the water

resistance of magnesium oxychloride cement (MOC), Constr. Build. Mater. 147 (2017) 519–524. doi:10.1016/J.CONBUILDMAT.2017.04.187.

[52] Z. Chen, J.-S. Li, B.-J. Zhan, U. Sharma, C.S. Poon, Compressive strength and microstructural properties of dry-mixed geopolymer pastes synthesized from GGBS and sewage sludge ash, Constr. Build. Mater. 182 (2018) 597–607. doi:10.1016/J.CONBUILDMAT.2018.06.159.

[53] M. Oliva, F. Vargas, M. Lopez, Designing the incineration process for improving the cementitious performance of sewage sludge ash in Portland and blended cement systems, J. Clean. Prod. 223 (2019) 1029–1041. doi:10.1016/J.JCLEPRO.2019.03.147.

[54] D. Vouk, D. Nakic, N. Stirmer, C. Cheeseman, Influence of combustion temperature on the performance of sewage sludge ash as a supplementary cementitious material, J. Mater. Cycles Waste Manag. 20 (2018) 1458–1467. doi:10.1007/s10163-018-0707-8.

[55] M. Liu, Y. Zhao, Y. Xiao, Z. Yu, Performance of cement pastes containing sewage sludge ash at elevated temperatures, Constr. Build. Mater. 211 (2019) 785–795. doi:10.1016/J.CONBUILDMAT.2019.03.290.

[56] G. Rutkowska, P. Wichowski, J. Fronczyk, M. Franus, M. Chalecki, Use of fly ashes from municipal sewage sludge combustion in production of ash concretes, Constr. Build. Mater. 188 (2018) 874–883. doi:10.1016/J.CONBUILDMAT.2018.08.167.

[57] K. De Weerdt, M. Ben Haha, G. Le Saout, K.O.O. Kjellsen, H. Justnes, B. Lothenbach, Hydration mechanisms of ternary Portland cements containing limestone powder and fly ash, Cem. Concr. Res. 41 (2011) 279–291. doi:10.1016/j.cemconres.2010.11.014.

[58] T. Matschei, B. Lothenbach, F.P. Glasser, The AFm phase in Portland cement, Cem. Concr. Res. 37 (2007) 118–130. doi:10.1016/J.CEMCONRES.2006.10.010.

[59] B. Lothenbach, G. Le Saout, E. Gallucci, K. Scrivener, Influence of limestone on the hydration of Portland cements, Cem. Concr. Res. 38 (2008) 848–860. doi:10.1016/J.CEMCONRES.2008.01.002.

[60] W. Piasta, M. Lukawska, The Effect of Sewage Sludge Ash on Properties of Cement Composites, Procedia Eng. 161 (2016) 1018–1024. doi:10.1016/j.proeng.2016.08.842.

[61] K.L. Scrivener, A. Nonat, Hydration of cementitious materials, present and future, Cem. Concr. Res. 41 (2011) 651–665. doi:10.1016/J.CEMCONRES.2011.03.026.

[62] P. Bénard, S. Garrault, A. Nonat, C. Cau-Dit-Coumes, Hydration process and rheological properties of cement pastes modified by orthophosphate addition, J. Eur. Ceram. Soc. 25 (2005) 1877–1883. doi:10.1016/J.JEURCERAMSOC.2004.06.017.

[63] W. Ma, P.W. Brown, Effect of phosphate additions on the hydration of Portland cement, Adv. Cem. Res. 6 (1994) 1–12. doi:10.1680/adcr.1994.6.21.1.

[64] C. Cau Dit Coumes, S. Courtois, Cementation of a low-level radioactive waste of complex chemistry: Investigation of the combined action of borate, chloride, sulfate and phosphate on cement hydration using response surface methodology, Cem. Concr. Res. 33 (2003) 305–316. doi:10.1016/S0008-8846(02)00943-2.

[65] P. Bénard, S. Garrault, A. Nonat, C. Cau-dit-Coumes, Influence of orthophosphate ions on the dissolution of tricalcium silicate, Cem. Concr. Res. 38 (2008) 1137–1141. doi:10.1016/J.CEMCONRES.2008.03.019.

[66] J. Skibsted, H.J. Jakobsen, Characterization of the Calcium Silicate and Aluminate Phases in Anhydrous and Hydrated Portland Cements by 27Al and 29Si MAS NMR Spectroscopy, in: Nucl. Magn. Reson. Spectrosc. Cem. Mater., Springer Berlin Heidelberg, Berlin, Heidelberg, 1998: pp. 3–45. doi:10.1007/978-3-642-80432-8_1.

[67] G.K. Sun, J.F. Young, R.J. Kirkpatrick, The role of Al in C–S–H: NMR, XRD, and compositional

results for precipitated samples, Cem. Concr. Res. 36 (2006) 18–29. doi:10.1016/J.CEMCONRES.2005.03.002.

[68] M.D. Andersen, H.J. Jakobsen, J. Skibsted, A new aluminium-hydrate species in hydrated Portland cements characterized by 27Al and 29Si MAS NMR spectroscopy, Cem. Concr. Res. 36 (2006) 3–17. doi:10.1016/J.CEMCONRES.2005.04.010.

[69] M.R. Jones, D.E. Macphee, J.A. Chudek, G. Hunter, R. Lannegrand, R. Talero, S.N. Scrimgeour, Studies using 27Al MAS NMR of AFm and AFt phases and the formation of Friedel's salt, Cem. Concr. Res. 33 (2003) 177–182. doi:10.1016/S0008-8846(02)00901-8.

[70] S. Joseph, J. Skibsted, Ö. Cizer, A quantitative study of the C3A hydration, Cem. Concr. Res. 115 (2019) 145–159. doi:10.1016/J.CEMCONRES.2018.10.017.

[71] P. Faucon, T. Charpentier, D. Bertrandie, A. Nonat, J. Virlet, J.C. Petit, Characterization of calcium aluminate hydrates and related hydrates of cement pastes by 27Al MQ-MAS NMR, Inorg. Chem. 37 (1998) 3726–3733.

[72] H.-J. Kuzel, H. Pöllmann, Hydration of C3A in the presence of Ca(OH)2, CaSO4·2H2O and CaCO3, Cem. Concr. Res. 21 (1991) 885–895. doi:10.1016/0008-8846(91)90183-I.

[73] M. Heikal, H. El-Didamony, M.S. Morsy, Limestone-filled pozzolanic cement, Cem. Concr. Res. 30 (2000) 1827–1834. doi:10.1016/S0008-8846(00)00402-6.

[74] M. Saillio, V. Baroghel-Bouny, M. Bertin, S. Pradelle, J. Vincent, Phase assemblage of cement pastes with SCM at different ages, Constr. Build. Mater. 224 (2019) 144–157. doi:10.1016/J.CONBUILDMAT.2019.07.059.

[75] I. Pane, W. Hansen, Investigation of blended cement hydration by isothermal calorimetry and thermal analysis, Cem. Concr. Res. 35 (2005) 1155–1164. doi:10.1016/j.cemconres.2004.10.027.

[76] H.L. Jang, H.K. Lee, K. Jin, H.Y. Ahn, H.E. Lee, K.T. Nam, Phase transformation from hydroxyapatite to the secondary bone mineral, whitlockite, J. Mater. Chem. B. 3 (2015) 1342–1349. doi:10.1039/c4tb01793e.

[77] T. Matschei, B. Lothenbach, F.P. Glasser, The role of calcium carbonate in cement hydration, Cem. Concr. Res. 37 (2007) 551–558. doi:10.1016/j.cemconres.2006.10.013.

[78] D. Damidot, B. Lothenbach, D. Herfort, F.P. Glasser, Thermodynamics and cement science, Cem. Concr. Res. 41 (2011) 679–695. doi:10.1016/J.CEMCONRES.2011.03.018.